

# Universal Non-equilibrium Response Theory Beyond Steady States

Jiming Zheng\* and Zhiyue Lu†

Department of Chemistry, University of North Carolina-Chapel Hill, NC

(Dated: October 25, 2024)

Fluctuation-dissipation relations elucidate the response of near-equilibrium systems to environmental changes, with recent advances extending response theory to non-equilibrium steady states. However, a general response theory for systems evolving far from steady states has remained elusive. Using information geometry of stochastic trajectory probabilities, we derive universal thermodynamic bounds on both linear and nonlinear responses of Markov systems to environmental changes, applicable across all non-equilibrium regimes. This theory establishes a new paradigm in non-equilibrium statistical mechanics, offering a unified perspective on the responsiveness of non-stationary systems to external control and environmental changes. Applicable to systems ranging from biological sensory processes to engineered responsive materials, our framework paves the way for understanding and designing complex responsiveness in far-from-equilibrium stochastic systems.

*Introduction.*—Beyond thermal equilibrium, biological and chemical systems demonstrate complex responsiveness to the changes of its surroundings. Unraveling the principles governing the sensitivity and robustness of systems toward external perturbations is crucial for understanding and designing life-like behaviors in complex systems. While the linear response theory near equilibrium [1, 2] captures the response of systems toward perturbations near thermal equilibrium. In the past few decades, there have been attempts to extend the linear response theory beyond thermal equilibrium, including violation of fluctuation-dissipation relation [3, 4], results obtained under Gaussian approximation [5], generalization of Einstein relation [6], and many other works [7–11]. Yet, there is still a gap between exact formal response theories and the tangible dynamical properties of systems. Recently, two groups have made prominent results in deriving intuitive bounds on the non-equilibrium responsiveness of stochastic systems [12–14]. However, these recent intuitive results are only applicable to systems restricted to the non-equilibrium steady states (NESS), which can not capture a system’s transient response beyond stationary. Today, a general framework for understanding the responsiveness of systems far from NESS remains elusive.

In this work, we present a set of universal response relations, Eqs. (6) to (8) and (10) for both linear and nonlinear responses of non-equilibrium systems. Here *linear response* refers to the response toward infinitesimally small changes of its surroundings, whereas *non-linear response* refers to system’s response toward large-amplitude stimuli. In both cases, our theory is applicable to systems that evolves arbitrarily far from NESS. Moreover, this theory explicitly relates a system’s responsiveness to its kinetic properties, providing direct insight into how dynamical characteristics governs the sensitivity to environmental conditions. This universal theory has the potential to transform our understanding of complex responsiveness of non-equilibrium systems and pave the way for the design of rich response features, such as sensitivity [15–17], adaptation [18–20], and

robustness [21–25], into far-from-equilibrium systems.

The key of the new theory is the construction of information geometry [26–29] in the space of Markovian trajectory probability distributions. Our approach differs from previous information-geometry thermodynamic theories [28, 29] by focusing on trajectory probabilities [30] instead of state probabilities. This novel perspective enables the theory to describe systems evolving far from steady states, significantly expanding the scope of response theory to non-equilibrium and non-stationary relaxation processes.

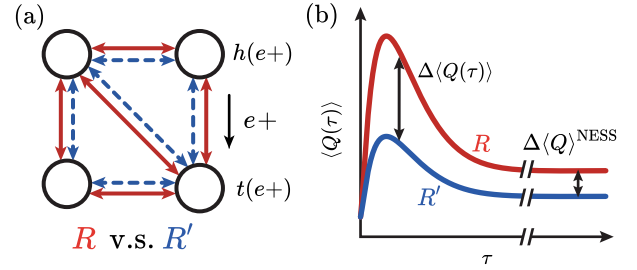


FIG. 1. (a) Markov system illustrated by a graph, where the transition of each directed edge (e.g.,  $e+$ ) jumps from the head vertex  $h(e+)$  to the tail  $t(e+)$ . (b) System’s response to an external change is quantified by comparing the dynamics of the original system  $R$  with the changed system  $R'$ . The transient response is captured by  $\Delta\langle Q(\tau) \rangle = |\langle Q[X_\tau] \rangle' - \langle Q[X_\tau] \rangle|$ , where  $Q(\tau)$  represents a time-dependent observable. As  $\tau \rightarrow \infty$ , both systems approach their respective NESS, and the response converges to  $\Delta\langle Q \rangle^{\text{NESS}}$ .

*Setup.*—Consider a Markov process described by a graph  $\mathbb{G} = (\{v_v\}, \{e_e\})$  with  $N_v$  vertices  $\{v_v\}$  and  $N_e$  undirected edges  $\{e_e\}$ . One can assign each edge  $e_e$  a forward and a reverse direction, with their corresponding transition probability rates denoted by  $(R_{e+}, R_{e-})$ . These rates can be alternatively denoted by the two vertices of the edge – the transition rate from  $v'$  to  $v$  is  $R_{e+} = R_{vv'}$ , and equivalently  $R_{e-} = R_{v'v}$ . Here we call the  $v'$  the head of the forward edge:  $h(e+) = v'$  and  $v$  the tail of the forward edge  $t(e+) = v$ , as shown in Fig. 1b.

The dynamics of the Markov system are represented by the master equation

$$\frac{d\mathbf{p}(t)}{dt} = R \cdot \mathbf{p}(t), \quad (1)$$

where  $\mathbf{p}(t) = (p_1(t), \dots, p_{N_v}(t))^T$  is the column vector of probability distributions on vertices at time  $t$  and  $R = \{R_{vv'}\}_{N_v \times N_v}$  is the rate matrix with diagonal elements  $R_{vv} = -\sum_{v', v' \neq v} R_{v'v}$ .

For a Markov system under the influence of external input or environmental conditions, its transition rates can be dependent on the control parameters (or environmental parameters). To generally describe this dependence, we denote the rate matrix  $R(\boldsymbol{\xi})$  as a function of all external control parameters:

$$\boldsymbol{\xi} = (\xi_1, \dots, \xi_{N_p})^T \quad (2)$$

which is a column vector with  $N_p$  control parameters. Examples of environmental parameters  $\xi_i$  include but are not limited to temperature, pressure, pH, chemical concentration, electric field, etc. Under this description, alternation in the control parameter  $\boldsymbol{\xi}$  changes the system's probability transition rates  $R(\boldsymbol{\xi})$ , which may result in changes in its dynamics.

To construct a theoretical framework for system's environmental responsiveness, especially if the system evolve in time rather than maintaining the NESS, we focus on the system's probability distribution stochastic trajectories. The trajectory distribution contains more information [30] than the solution of the master equation – state probability  $\mathbf{p}(t)$ . Here, a trajectory with time length  $\tau$  can be denoted by a sequence of  $n$  jump events at time  $\{t_i\}$ :

$$X_\tau = ((x_0, t_0), (x_1, t_1), \dots, (x_n, t_n)), \quad (3)$$

where  $x_i \in \{\mathbf{v}_v\}$ , the initial time is denoted by  $t_0 = 0$ , and  $t_n \leq \tau$  is the time when the last jump occurs before  $\tau$ . The probability of the trajectory  $X_\tau$  can be represented by the following product,  $\mathcal{P}[X_\tau] = \mathcal{P}[X_\tau|x_0] \cdot p_{x_0}(0)$  where  $p_{x_0}(0)$  is the initial state probability and  $\mathcal{P}[X_\tau|x_0]$  is the conditional path probability of  $X_\tau$  given the initial state  $x_0$ . The conditional path probability can also be represented by [31]

$$\mathcal{P}[X_\tau|x_0] = \prod_{i=1}^n R_{x_i x_{i-1}} \prod_{i=0}^n e^{\int_{t_i}^{t_{i+1}} R_{x_i x_i} dt}, \quad (4)$$

where  $t_{n+1} = \tau$  is the time length of the trajectory.

The central result of this letter is the environmental responsiveness of Markov systems without the restriction of NESS. Without losing generality, the environmental change can be arbitrary alternations of  $\boldsymbol{\xi}$  and the response can be denoted by the trajectory-averaged changes of arbitrary observable  $\langle Q[X_\tau] \rangle$ . Here the angular brackets denote an average over the ensemble of

trajectories generated from the Markov dynamics  $R(\boldsymbol{\xi})$ . We consider system's response toward two types of environmental changes: (1) *perturbative change* or *linear response*,  $|\partial_{\xi_p} \langle Q(\tau) \rangle|$ , which captures the infinitesimal change of the non-stationary observable caused by the infinitesimal environmental perturbation, and (2) *finite change* or *nonlinear response*,  $\Delta \langle Q(\tau) \rangle = |\langle Q(\tau) \rangle' - \langle Q(\tau) \rangle|$ , which quantifies the difference in the system's non-stationary outputs between two finitely different environmental conditions  $\boldsymbol{\xi}'$  and  $\boldsymbol{\xi}$ .

*Information Geometry.*—To build a general theory, we construct information geometry [26, 27] for the space of trajectory probabilities, where the Fisher information metric is chosen as the metric tensor for the parametric probability distributions.

Given a Markov graph and an initial state distribution  $\mathbf{p}(0)$ , the rate matrix  $R(\boldsymbol{\xi})$  fully determines the trajectory probability distribution conditioned by the initial  $\mathbf{p}(0)$ . This correspondence between the rate matrix and conditional path probability is shown by Fig. 2(a) and (b). As a result, the manifold  $\mathcal{M}_{\mathcal{P}|p_0}$  of conditional path probabilities  $\mathcal{P}[X_\tau|x_0]$ , as shown by Fig. 2(c), can be fully represented by transition rate matrix  $R$ . Since the degree of freedom for  $R$  is  $2N_e$ , the resulting conditional path probability manifold  $\mathcal{M}_{\mathcal{P}|p_0}$  is  $2N_e$ -dimensional. In other words, Fig. 2(a) and (c) share the same dimensionality, and every point on the manifold uniquely specifies an evolution process (i.e., a distribution of trajectories). One can alternatively represent the conditional path probability manifold by embedding it on a hypersphere of radius 2 [27], illustrated by Fig. 2(d). The hypersphere representation provides a geometric argument for the nonlinear responsiveness relation.

As mentioned above, the natural and complete choice of the coordinate system for the  $2N_e$ -dimension manifold  $\mathcal{M}_{\mathcal{P}|p_0}$  is the set of all transition rates  $\{R_{e+}\} \cup \{R_{e-}\}$ . We refer to this choice as *transition rate coordinates*. With the help of the trajectory KL divergence recently derived in [30], one immediately obtains the *geometric foundation* of this work – the Fisher information metric:

$$g(\{R_{e+}\}, \{R_{e-}\}) = \text{diag} \left\{ \left\{ \frac{\mathcal{A}_{e+}}{R_{e+}^2} \right\}, \left\{ \frac{\mathcal{A}_{e-}}{R_{e-}^2} \right\} \right\}. \quad (5)$$

where  $\mathcal{A}_{e+} = \int_0^\tau R_{e+} p_{h(e+)}(t) dt$  denotes the *directed activity* (i.e. time-integrated direct traffic) on the directed edge  $e+$  [32]. The directed activity is the expectation value of the number of directed transitions along edge  $e+$  within the time duration  $\tau$  [33], which was shown to play an important role in various thermodynamic relations by recent studies [11, 34–38]. Notice that the above metric tensor is globally diagonal, which implies that the transition rate coordinate system serves as orthogonal basis everywhere. The metric under other coordinate systems (e.g., the explicit environmental parameter coordinate system  $\boldsymbol{\xi}$ ) can be obtained through coordinate

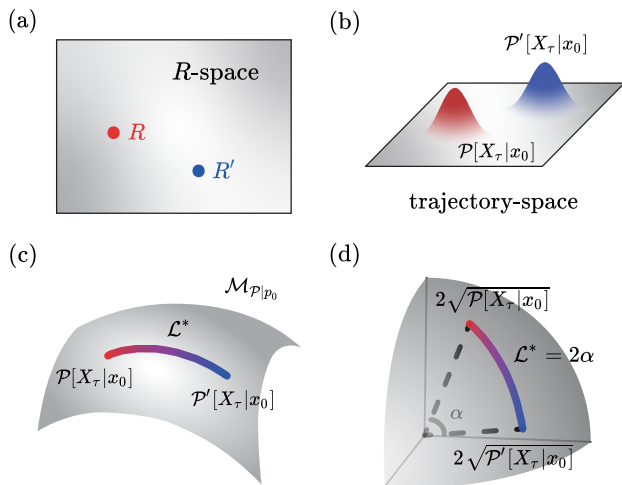


FIG. 2. Four spaces to represent Markov Processes. (a) The space of rate matrices, where the original and changed dynamics are shown by two points. (b) In the trajectory space, two probability distributions of trajectories conditioned by initial distribution  $\mathbf{p}(0)$  are sketched, and they are generated by the two Markov dynamics ( $R$  or  $R'$ ). (c) The two distributions  $\mathcal{P}[X_\tau|x_0]$  and  $\mathcal{P}'[X_\tau|x_0]$  are represented by two points on the manifold  $\mathcal{M}_{\mathcal{P}|p_0}$ . The shortest path between them is the geodesic  $\mathcal{L}^*$ . (d) The manifold  $\mathcal{M}_{\mathcal{P}|p_0}$  is isometrically embedded to the positive orthant of a radius-2 hypersphere of dimension  $2N_e$ , thus the geodesic length between two points becomes an arc length  $\mathcal{L}^* = 2\alpha$ .

transformations. Taking advantage of the orthogonality of the transition rate basis, it is straightforward to define and evaluate various geometric quantities on the manifold. For example, the line element  $ds^2$  in terms of transition rates is then given by  $ds^2 = \sum_{e\pm} \frac{A_{e\pm}}{R_{e\pm}^2} dR_{e\pm}^2$ . For an infinitesimal displacement along any axis of the transition rate coordinates, e.g.,  $R_{e+}$ , the line element is simply  $ds^2 = \frac{A_{e+}}{R_{e+}^2} dR_{e+}^2$ . The geodesic between any two points on the manifold is the path of minimum curve length, illustrated by  $\mathcal{L}^*$  in two representations of the manifold Fig. 2(c) and (d).

Within the general framework of information geometry, this work describes system's non-stationary responses to both perturbative and finite environmental changes, i.e., (1) linear response beyond stationarity and (2) nonlinear response relations.

*Linear Response Beyond Stationarity.*—By applying the Cramér-Rao inequality [39, 40] to the trajectory Fisher information metric defined in Eq. (5), we obtain the *first central result* of this work: the thermodynamic bound for the response magnitude of any observable  $Q$  to the perturbation. The result takes two forms. When considering system's response to the perturbation of a single transition rate, the responsiveness relation can be

expressed by:

$$\left| \frac{\partial \langle Q(\tau) \rangle}{\partial R_{e\pm}} \right| \leq \sqrt{\text{Var}[Q]} \cdot \frac{\sqrt{A_{e\pm}}}{R_{e\pm}}, \quad (6)$$

where the only change is applied to a single directed edge  $R_{e+}$  (or  $R_{e-}$ ), while all other transition rates remain intact. Here the expectation value of the observable is the ensemble average over all stochastic trajectories of time-length  $\tau$ :  $\langle Q(\tau) \rangle = \int \mathcal{D}[X_\tau] \mathcal{P}[X_\tau] Q[X_\tau]$ . Under different choices of the exact form for  $Q[X_\tau]$ , the definition can generally represent either a trajectory observable (time accumulated quantity) or a transient observable. To realize a transient observable at any time  $t$ , one can introduce a delta function peaked at time  $t$  into  $Q[X_\tau]$ . Formal discussions on different types of transient observables and their corresponding numerical results can be found in SI.II. If one chooses  $Q[X_\tau]$  as a time accumulation observable, our response relations can provide NESS response relations.

In general, Eq. (6) implies that the responsiveness of an observable is bounded by the product between the square root of observable variance  $\text{Var}[Q] \equiv \langle Q(\tau)^2 \rangle - \langle Q(\tau) \rangle^2$  and the square root of the scaled dynamical activity of the perturbed transition rates. Also, in alignment with intuition, this result indicated that the directed edge with larger activities may result in a stronger response toward the perturbation of its rate.

More conveniently, the above response relation can be formulated in terms of environmental-variable responsiveness relation. Through coordinate transformation into the environmental coordinate  $\xi$  in Eq. (2), the responsiveness bound to any chosen environmental variable change  $\delta\xi_i$  can be obtained:

$$\left| \frac{\partial \langle Q \rangle}{\partial \xi_i} \right| \leq \sqrt{\text{Var}[Q]} \cdot \sqrt{\sum_{e\pm} \frac{A_{e\pm}}{R_{e\pm}^2} \left( \frac{\partial R_{e\pm}}{\partial \xi_i} \right)^2}, \quad (7)$$

where  $\frac{\partial R_{e\pm}}{\partial \xi_i}$  denotes the transition rate's dependence on the environmental variable  $\xi_i$  while fixing all other environmental conditions. An illustrative example of the application of this relation to illustrate the system's environmental responsiveness can be found in the example at the end of this letter. More formal analysis on the change of coordinate system to study system's responses to dissipative thermodynamic driving forces can also be found in SI.III.

*Nonlinear Responsiveness Relations.*—Based on the geometry of the whole manifold  $\mathcal{M}_{\mathcal{P}|p_0}$ , we can obtain the *second central result*, universal responsiveness relations toward finite environmental condition change  $\xi$  to  $\xi'$ . For comparison, the linear-responsiveness relations only utilizes local geometric property of the manifold.

First, the following *geometric non-linear responsive-*

ness relation holds:

$$\arctan \frac{|\langle Q(\tau) \rangle' - \langle Q(\tau) \rangle|}{\sqrt{\text{Var}[Q]} + \sqrt{\text{Var}'[Q]}} \leq \frac{\mathcal{L}^*(\tau)}{2} \leq \frac{\mathcal{L}(\tau)}{2}, \quad (8)$$

where the  $\mathcal{L}^*$  is the geodesic length between the two path distributions for the two environmental conditions  $\xi$  and  $\xi'$ . Geometrically, the ratio  $\mathcal{L}^*/2 = \alpha$  is the angle shown in Fig. 2(d); and the second inequality in Eq. (8) comes from the fact that the geodesic length  $\mathcal{L}^*$  is shorter than any other curve length  $\mathcal{L}$ . Here we define a curve length  $\mathcal{L}$  by accumulated difference on all the changed rates:

$$\mathcal{L}(\tau) = \int_R^{R'} \sqrt{\sum_{e\pm} \frac{A_{e\pm}}{R_{e\pm}^2} (dR_{e\pm})^2}. \quad (9)$$

By combining Eqs. (8) and (9) and Jensen's inequality [41], one can further obtain an alternative *dynamical nonlinear responsiveness relation* that *explicitly reveals* the connection between system's responsiveness and its dynamical rate changes:

$$\arctan \frac{|\langle Q(\tau) \rangle' - \langle Q(\tau) \rangle|}{\sqrt{\text{Var}[Q]} + \sqrt{\text{Var}'[Q]}} \leq \sum_{e\pm} \left| \sqrt{R'_{e\pm}\tau} - \sqrt{R_{e\pm}\tau} \right|. \quad (10)$$

The geometric and dynamical nonlinear responsiveness relations, Eqs. (8) and (10), reveal that the difference between two Markov system dynamics, reflected by an observable  $Q[X_\tau]$ , is geometrically bounded by an angle  $\alpha$  (see Fig. 2(d)), and is explicitly bounded by the total square-root-rate differences of all edges. This geometric argument is elaborated below.

*Geometric Proof of Nonlinear Response Relation.*— Let us consider alternative representations of the space of conditional trajectory probabilities as illustrated by Fig. 2. Notice that each trajectory probability density  $\mathcal{P}[X_\tau; R]$  is a map from the product space of the Hilbert space of trajectories  $\Omega$  and the  $2N_e$  dimensional rate parameter space  $\Xi$  to a positive real number, i.e.,  $\mathcal{P}[X_\tau; R] : \Omega \times \Xi \rightarrow \mathbb{R}^+$ . For two different rate matrices  $R$  and  $R'$ , the corresponding trajectory densities are represented by  $\mathcal{P} \equiv \mathcal{P}[X_\tau; R]$  and  $\mathcal{P}' \equiv \mathcal{P}[X_\tau; R']$ . Inspired by reference [27], we define their corresponding  $\theta$ -scaled half density via a map  $\pi_\theta^{1/2} : \mathcal{P} \mapsto \rho \equiv \theta\sqrt{\mathcal{P}}$  with a positive real number  $\theta$ . Here  $\pi_\theta^{1/2}$  is a diffeomorphism and preserves the geodesic.

The map  $\pi_\theta^{1/2}$  provides us with an alternative representation of the trajectory probability manifold  $\mathcal{M}_{\mathcal{P}|p_0}$  with fisher information metric as a hypersphere in Euclidean space with radius  $\theta$ . In the half-density representation, the inner product is defined by integrating over the trajectory Hilbert space  $\Omega$ :

$$(\rho, \rho') = \int \rho \rho' \mathcal{D}[X_\tau], \quad (11)$$

Thus, due to normalization over trajectory space  $\Omega$ , the self inner product for each  $\rho$  must be  $(\rho, \rho) \equiv \|\rho\|^2 = \theta^2$ . In other words, all  $\rho$ 's lives on the positive orthant of the radius- $\theta$  hypersphere of dimension  $2N_e$  as shown in Fig. 2(d).

By choosing  $\theta = 2$ , the map  $\pi_2^{1/2}$  becomes a isometric diffeomorphism. In other words, the geodesic length on the hypersphere between  $\rho$  and  $\rho'$  coincides with the geodesic length  $\mathcal{L}^*$  between  $\mathcal{P}$  and  $\mathcal{P}'$ . Geometrically, by representing the former as the arc length on the great circle with radius  $\theta = 2$ , we have  $\mathcal{L}^* = 2\alpha$ , where  $\alpha$  is the geodesic angle as shown in Fig. 2(d).

Under this geometric analysis, one can further obtain

$$\cos \alpha = \frac{(\rho, \rho')}{\|\rho\| \cdot \|\rho'\|} = \int_\Omega \sqrt{\mathcal{P}} \sqrt{\mathcal{P}'} \mathcal{D}[X_\tau]. \quad (12)$$

By combining this with the inequality for Hellinger distance from [42], we arrive at

$$\cos \alpha \leq \left[ \left( \frac{\langle Q(\tau) \rangle' - \langle Q(\tau) \rangle}{\sqrt{\text{Var}'[Q]} + \sqrt{\text{Var}[Q]}} \right)^2 + 1 \right]^{-1/2}. \quad (13)$$

By rearrangements, we can obtain the non-linear response inequality Eq. (8). More details of the derivation can be found in SI.IV-A.

From this geometry perspective, one can consider the nonlinear response relations, Eqs. (8) and (10), as extensions of the linear response relation, Eq. (6). The non-linear relation reduces to the linear case in the limit of  $R' \rightarrow R$ . In this case, the geodesic shrinks to a point and the geodesic length  $\mathcal{L}^*$  reduces to the local Fisher information metric, Eq. (5), and the linear-response relation Eqs. (6) and (7) is recovered.

*Discussion: Information Geometry Framework.*— This new geometric framework is inherently different from the previous results [28, 29, 43, 44], which was developed with the manifold of the probability distributions of states,  $\mathcal{M}_p$ . The uniqueness of the new framework is the construction of information geometry on the manifold of conditional distribution of trajectories,  $\mathcal{M}_{\mathcal{P}|p_0}$ . These two manifolds can be connected by the construction of the complete trajectory probability distribution manifold,  $\mathcal{P}[X_\tau]$ , which is locally the product manifold  $\mathcal{M}_p \times \mathcal{M}_{\mathcal{P}|p_0}$ . The metric for the manifold  $\mathcal{P}[X_\tau]$  is the product metric  $g_p \oplus g_{\mathcal{P}|p_0}$ . It is noteworthy that, in our analysis for trajectory probability manifolds, one does not need to include the trajectory length  $\tau$  as a parameter. It is because the rates ( $\{R_{e+}\} \cup \{R_{e-}\}$ ) and the time length  $\tau$  are dependent on each other under an equivalence relation shown in the recent work [35, 45]. With the equivalence property, one can reduce our results Eqs. (6) and (8) to the previously discovered uncertainty relations in terms of system's dynamical activity in [35, 45] by rescaling all transition rates by a same factor.

We here conjecture that the responsiveness inequality may be better saturated when the observable  $Q$  is strongly correlated with the transition events of the perturbed edge, as is illustrated in the End Matter. More technical discussions of the saturation condition for the inequalities are provided in SI.V.

Notice that the local geometric property of the trajectory manifold, Eq. (5), obtained by the Fisher information of classical Markov trajectories, agrees with previous works on the quantum Fisher information for Lindblad equation [46, 47]. In the future, it is useful to explore if the information geometric framework developed for classical Markov systems in this work, especially the nonlinear responsiveness relations, Eqs. (8) and (10), can be extended by considering quantum information geometry approaches [48].

*Application: Responsiveness Design Principle.*—Our responsiveness relation provides a general theoretical principle to guide the design of a system’s non-stationary response to environmental condition changes. This relation connects experimentally accessible measurements (observable  $Q$ ) with system’s inherent transition statistics:

$$\eta_i^Q \equiv \frac{(\partial_{\xi_i} \langle Q \rangle)^2}{\text{Var}[Q]} \leq \mathcal{A} \cdot \sum_{e\pm} a_{e\pm}^2(\xi_i) \frac{\mathcal{A}_{e\pm}}{\mathcal{A}} \quad (14)$$

$$= \mathcal{A} \cdot \overline{a_i^2} \equiv \eta_i^{\text{Bound}}, \quad (15)$$

where  $\eta_i^Q$  denotes the sensitivity-to-noise ratio for observable  $Q$  with respect to control parameter  $\xi_i$ ,  $a_{e\pm}(\xi_i) \equiv \partial_{\xi_i} \ln R_{e\pm}$  is the *logarithm sensitivity* of each transition’s rate with respect to the control variable  $\xi_i$ ,  $\mathcal{A}$  is the total activity,  $\mathcal{A}_{e\pm}/\mathcal{A}$  is the fraction of transitions from each edge, and  $\overline{a_i^2}$  is the statistical average of the *logarithm rate sensitivity* for all observed transition events. This result aligns with intuition: the parameter sensitivity of a non-equilibrium process depends on the total activity  $\mathcal{A}$  and the average logarithmic rate sensitivity of observed transitions. By further choosing observational time scale to maintains a constant activity  $\mathcal{A}$ , system’s sensitivity only depends on the average logarithmic rate sensitivity of observed edges,  $\overline{a_i^2}$ .

This result can be illustrated with a thermal system described by the generalized Arrhenius law

$$R_{e\pm} = C_e e^{-\beta(B_e - E_{h(e\pm)}) + \beta w_{e\pm}}, \quad (16)$$

where  $\beta = 1/k_B T$  is the inverse temperature,  $B_e$  denotes energy barrier for edge  $e$ ,  $C_e$  and  $c_e$  are constants for edge  $e$ ,  $E_{h(e\pm)}$  denotes the energy of the head of the directed transition edge  $e\pm$ , and  $w_{e\pm}$  denotes the non-equilibrium work applied to assist transition  $e\pm$  that breaks the detailed balance. In this case, the logarithm rate sensitivity for inverse temperature is the generalized activation energy  $a_{e\pm} = w_{e\pm} - (B_e - E_{h(e\pm)})$ . To design a system with ultra-low (or high) temperature sensitivity, one needs to

minimize (or maximize)  $\eta_i^{\text{Bound}}$  via optimizing the energy landscapes and the external driving patterns. Moreover, to create a system sensitive to one variable ( $\xi_i$ ) but robust to another ( $\xi_j$ ), one can focus on maximizing the ratio between their respective sensitivity bounds  $\eta_i^{\text{Bound}}/\eta_j^{\text{Bound}}$ .

*Conclusion.*—In summary, this work presents a set of universal responsiveness relations for non-stationary Markov processes under either infinitesimal or finite-amplitude perturbations. These relations explicitly reveal the connection between any observable’s environmental response, the variance of the measured observable and the dynamical features of the system. It provide a powerful tool for understanding and predicting the environmental responsiveness of complex systems far from equilibrium, with a wide range of potential applications in biological sensory processes and synthetic responsive materials. The illustrative example reveals that the explicit responsiveness relations presented in this work may lead to practical design principles to help the design and optimization of stochastic sensors, biological or synthetic, with desired time-dependent sensitivity or robustness.

*Acknowledgments.*—This work is funded by National Science Foundation Grant DMR-2145256. The authors appreciate discussions and suggestions on the manuscript from Prof. Chris Jarzynski and from attendees at the Frontiers of Non-equilibrium Physics 2024 workshop held in July 2024 at Kyoto University, Japan.

---

\* jiming@unc.edu

† zhiyuelu@unc.edu

- [1] R. Kubo, The fluctuation-dissipation theorem, Reports on progress in physics **29**, 255 (1966).
- [2] R. Kubo, Statistical-mechanical theory of irreversible processes. i. general theory and simple applications to magnetic and conduction problems, Journal of the physical society of Japan **12**, 570 (1957).
- [3] T. Harada and S. Shin-ichi, Equality connecting energy dissipation with a violation of the fluctuation-response relation, Physical review letters **95**, 130602 (2005).
- [4] C. Maes and M. H. van Wieren, Time-symmetric fluctuations in nonequilibrium systems, Physical review letters **96**, 240601 (2006).
- [5] K. Sato, Y. Ito, T. Yomo, and K. Kaneko, On the relation between fluctuation and response in biological systems, Proceedings of the National Academy of Sciences **100**, 14086 (2003).
- [6] M. Baiesi, C. Maes, and B. Wynants, The modified sutherland–einstein relation for diffusive non-equilibria, Proceedings of the Royal Society A: Mathematical, Physical and Engineering Sciences **467**, 2792 (2011).
- [7] C. Maes and B. Wynants, On a response formula and its interpretation, arXiv preprint arXiv:0910.2320 (2009).
- [8] P. E. Harunari, S. Dal Cengio, V. Lecomte, and M. Poletini, Mutual linearity of nonequilibrium network currents, Phys. Rev. Lett. **133**, 047401 (2024).
- [9] A. Dechant and S.-i. Sasa, Fluctuation–response inequality out of equilibrium, Proceedings of the National

- Academy of Sciences **117**, 6430 (2020).
- [10] C. Maes, Response theory: a trajectory-based approach, *Frontiers in Physics* **8**, 229 (2020).
- [11] M. Baiesi, C. Maes, and B. Wynants, Fluctuations and response of nonequilibrium states, *Physical review letters* **103**, 010602 (2009).
- [12] J. A. Owen, T. R. Gingrich, and J. M. Horowitz, Universal thermodynamic bounds on nonequilibrium response with biochemical applications, *Physical Review X* **10**, 011066 (2020).
- [13] T. Aslyamov and M. Esposito, Nonequilibrium response for markov jump processes: Exact results and tight bounds, *Physical Review Letters* **132**, 037101 (2024).
- [14] T. Aslyamov and M. Esposito, A general theory of static response for markov jump processes, arXiv preprint arXiv:2402.13990 (2024).
- [15] T. Mora, Physical limit to concentration sensing amid spurious ligands, *Physical review letters* **115**, 038102 (2015).
- [16] W. Bialek and S. Setayeshgar, Physical limits to biochemical signaling, *Proceedings of the National Academy of Sciences* **102**, 10040 (2005).
- [17] D. Hartich, A. C. Barato, and U. Seifert, Sensory capacity: An information theoretical measure of the performance of a sensor, *Physical Review E* **93**, 022116 (2016).
- [18] B. Wark, B. N. Lundstrom, and A. Fairhall, Sensory adaptation, *Current opinion in neurobiology* **17**, 423 (2007).
- [19] G. Lan, P. Sartori, S. Neumann, V. Sourjik, and Y. Tu, The energy–speed–accuracy trade-off in sensory adaptation, *Nature physics* **8**, 422 (2012).
- [20] D. Conti and T. Mora, Nonequilibrium dynamics of adaptation in sensory systems, *Physical Review E* **106**, 054404 (2022).
- [21] C. S. Pittendrigh, On temperature independence in the clock system controlling emergence time in drosophila, *Proceedings of the National Academy of Sciences* **40**, 1018 (1954).
- [22] C. H. Johnson and M. J. Rust, *Circadian rhythms in bacteria and microbiomes*, Vol. 409 (Springer, 2021).
- [23] J. B. Hogenesch and H. R. Ueda, Understanding systems-level properties: timely stories from the study of clocks, *Nature Reviews Genetics* **12**, 407 (2011).
- [24] N. Ay and D. C. Krakauer, Geometric robustness theory and biological networks, *Theory in biosciences* **125**, 93 (2007).
- [25] H. Fu, C. Fei, Q. Ouyang, and Y. Tu, Temperature compensation through kinetic regulation in biochemical oscillators, arXiv preprint arXiv:2401.13960 (2024).
- [26] S.-i. Amari, *Information geometry and its applications*, Vol. 194 (Springer, 2016).
- [27] N. Ay, J. Jost, H. Vân Lê, and L. Schwachhöfer, *Information geometry*, Vol. 64 (Springer, 2017).
- [28] S. Ito, Stochastic thermodynamic interpretation of information geometry, *Physical review letters* **121**, 030605 (2018).
- [29] G. E. Crooks, Measuring thermodynamic length, *Physical Review Letters* **99**, 100602 (2007).
- [30] A. Pagare, Z. Zhang, J. Zheng, and Z. Lu, Stochastic distinguishability of Markovian trajectories, *The Journal of Chemical Physics* **160**, 171101 (2024).
- [31] U. Seifert, Stochastic thermodynamics, fluctuation theorems and molecular machines, *Reports on progress in physics* **75**, 126001 (2012).
- [32] For systems evolving under time-dependent rate matrix, the Fisher information is discussed in the S.I.I.
- [33] C. Maes, Frenesy: Time-symmetric dynamical activity in nonequilibria, *Physics Reports* **850**, 1 (2020).
- [34] J. P. Garrahan, Simple bounds on fluctuations and uncertainty relations for first-passage times of counting observables, *Physical Review E* **95**, 032134 (2017).
- [35] I. Di Terlizzi and M. Baiesi, Kinetic uncertainty relation, *Journal of Physics A: Mathematical and Theoretical* **52**, 02LT03 (2018).
- [36] N. Shiraishi, K. Funo, and K. Saito, Speed limit for classical stochastic processes, *Physical review letters* **121**, 070601 (2018).
- [37] P. E. Harunari, A. Dutta, M. Poletti, and É. Roldán, What to learn from a few visible transitions’ statistics?, *Physical Review X* **12**, 041026 (2022).
- [38] Y. Hasegawa, Thermodynamic correlation inequality, *Physical Review Letters* **132**, 087102 (2024).
- [39] C. R. Rao, Information and the accuracy attainable in the estimation of statistical parameters, in *Breakthroughs in Statistics: Foundations and basic theory* (Springer, 1992) pp. 235–247.
- [40] H. Cramér, *Mathematical methods of statistics*, Vol. 26 (Princeton university press, 1999).
- [41] J. L. W. V. Jensen, Sur les fonctions convexes et les inégalités entre les valeurs moyennes, *Acta mathematica* **30**, 175 (1906).
- [42] T. Nishiyama, A tight lower bound for the hellinger distance with given means and variances, arXiv preprint arXiv:2010.13548 (2020).
- [43] D. A. Sivak and G. E. Crooks, Thermodynamic metrics and optimal paths, *Physical review letters* **108**, 190602 (2012).
- [44] S. Ito, Geometric thermodynamics for the fokker–planck equation: stochastic thermodynamic links between information geometry and optimal transport, *Information Geometry* **7**, 441 (2024).
- [45] Y. Hasegawa, Unifying speed limit, thermodynamic uncertainty relation and heisenberg principle via bulk-boundary correspondence, *Nature Communications* **14**, 2828 (2023).
- [46] K. Macieszczak, M. Guță, I. Lesanovsky, and J. P. Garrahan, Dynamical phase transitions as a resource for quantum enhanced metrology, *Physical Review A* **93**, 022103 (2016).
- [47] J. P. Garrahan and M. Guță, private communication.
- [48] M. Guță and J. Kiukas, Information geometry and local asymptotic normality for multi-parameter estimation of quantum markov dynamics, *Journal of Mathematical Physics* **58** (2017).

## End Matter

*Appendix: Saturation of Responsiveness Inequalities.*—In this End Matter, we investigate conditions under which our responsiveness bounds approach saturation, focusing on a simple yet illustrative case: the linear response of state probability to rate perturbation in a three-state Markov system. The perturbative responsiveness inequality is given below

(also see Eq.(S10) from SI.II)

$$\left| \frac{\partial p_{v_i}}{\partial R_{e_{\pm}}} \right| \leq \sqrt{p_{v_i}(1-p_{v_i})} \cdot \frac{\sqrt{\mathcal{A}_{e_{\pm}}}}{R_{e_{\pm}}}. \quad (17)$$

The numerical illustration of the bound tightness for other types of observables can be found in SI.II, and the formal mathematical analysis on the bound saturation conditions of each responsiveness relations involved in this letter can be found in SI.V.

We study a three-state Markov system (Fig. 3(a)) where we observe the probability of state  $v_1$ ,  $p_{v_1}(t)$  while perturbing the transition rate  $R_{32}$  (from state  $v_2$  to  $v_3$ ). To systematically explore different dynamical regimes, we generated  $4^6$  different Markov models by assigning each of the six transition rates values from  $\{0.01, 0.1, 1, 10\}$ . Starting from an initial condition localized at state  $v_2$ , we computed the ratio of actual response to our theoretical bound,  $|\partial_{R_{32}} p_{v_1}(t)|/\text{Bound}(t)$ , for each model (Fig. 3(b)).

Remarkably, six cases achieve more than 90% of the theoretical bound (highlighted by colored dash lines in Fig. 3(b)). These high-saturation cases, despite falling into two distinct categories of fast and slow relaxation (Fig. 3(c) and (d)), share three key features: 1) The transition from the initial state  $v_2$  to the observed state  $v_1$  is dominated by the perturbed path due to the rate imbalance  $R_{32} \gg R_{12}$ . 2) The transition from state  $v_3$  to state  $v_1$  is significantly faster than any other transition in the graph, i.e.,  $R_{13} \gg 1$  is dominating over all other rates. 3) The Markov graphs all favor the observed state  $v_1$  as the final dominant state.

These rate features create an optimal pathway where probability flow from the initial state  $v_2$  to the final dominant state  $v_1$  must first traverse the perturbed edge  $R_{32}$  and then immediately reach the observed state  $v_1$  via the dominant edge  $R_{13}$ . This dynamics ensures that **(D1)**–The dominant pathway from the initial state to the observed state must traverse the perturbed edge. **(D2)**–Once the perturbed transition occurs, the system rapidly reaches the observed state, **(D3)**–The observed state accumulates sufficient probability for measurable response.

These dynamical features suggest general principles for when our responsiveness bounds may be tight. Based on the kinetic analysis above, we conjecture that the saturation of our responsiveness bounds requires two key conditions: **(C1)**–Strong statistical correlation between transitions along the perturbed edge and changes in the

observable. This is ensured by dynamical features **(D1)** and **(D2)**. **(C2)**–Sufficient sampling of the observable itself (in this case, accumulation of probability in the observed state). This is ensured by dynamical features **(D3)**.

The first condition, **(C1)**, is satisfied by the pathway architecture ( $R_{32} \gg R_{12}$  and large  $R_{13}$ ), which ensures that observable changes (increase of  $p_{v_1}$ ) are tightly coupled to the stochastic transitions occurred the perturbed edge. The second condition, **(C2)**, is met through the steady-state probability distribution being peaked at the observed state. This provides an intuitive understanding of bound saturation complementary to the mathematical analysis presented in SI.V. In future work, a rigorous proof of these conjectures and their implications for optimal sensor design will be explored.

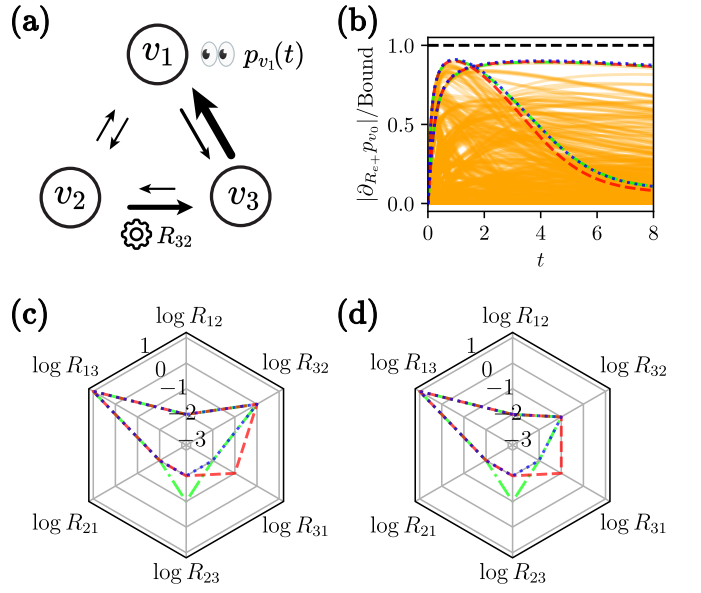


FIG. 3. Saturation analysis of responsiveness bound in a three-state Markov system. (a) Schematic of the three-state Markov system with transition rates  $R_{ij}$  between states  $v_i$  and  $v_j$ . The perturbed rate  $R_{32}$  and the observed state  $v_1$  are highlighted by a gear and a pair of eyes. (b) Time evolution of the response-to-bound ratio  $|\partial_{R_{32}} p_{v_1}(t)|/\text{Bound}(t)$  for  $4^6$  different rate matrices. Six cases achieving more than 90% of the theoretical bound are highlighted by colored dashed lines. The black dash line indicates the theoretical limit of all-time bound saturation. (c,d) Transition rates of the six high-saturation cases, showing fast relaxation (c) and slow relaxation (d) regimes. The rates are plotted on a logarithmic scale, revealing the key features of  $R_{32} \gg R_{12}$  and large  $R_{13} \gg 1$  common to all high-saturation cases.